Post-synthesis phase and shape evolution of $CsPbBr_3$ colloidal nanocrystals: the role of ligands

Elisabetta Fanizza,*‡[a,b] Francesca Cascella,‡[a†] Davide Altamura,[c] Cinzia Giannini,[c] Annamaria Panniello,[b] LeonardoTriggiani,[a,b] Nicoletta Depalo,[b] Angela Agostiano,[a,b] M. Lucia Curri[b] and Marinella Striccoli[b]

[a]Dipartimento di Chimica, Università degli Studi di Bari "A. Moro", Via Orabona 4 , 70126 Bari (IT)

[b]CNR-Istituto per i Processi Chimico Fisici, S. S. Bari, Via Orabona, 4, 70126 Bari (IT)

[c]CNR-Istituto di Cristallografia, Via Amendola, 122/O, 70126 Bari (IT).

† Present Address: Max Planck Institute for Dynamics of Complex Technical Systems, Physical and Chemical Foundations of Process Engineering, Sandtorstr.1, D-39106 Magdeburg, (DE)

‡ These authors contributed equally.

* corresponding author: elisabetta.fanizza@uniba.it; m.striccoli@ba.ipcf.cnr.it

Abstract. The surface chemistry of colloidal cesium lead bromide ($CsPbBr_3$) nanocrystals is decisive in determine the stability and the final morphology of this class of material, characterized by ionic structure and a high defect tolerance factor. Here, the high sensitivity of purified colloidal nanocubes of $CsPbBr_3$ to diverse environmental condition (solvent dilution, ageing, ligands post synthetic treatment) in ambient atmosphere is proved thanks to a comprehensive morphological (electron microscopy), structural (θ/2θ XRD and GIWAXS) and spectroscopic investigation. In particular, we establish the ability of aliphatic carboxylic acids and alkyl amines ligands to induce, even in a post preparative process at room temperature, structural, morphological and spectroscopic variations. Upon addition of oleyl amine the highly green emitting $CsPbBr_3$ nanocubes effectively turn into 1D thin tetragonal nanowires or lead halide deficient rhombohedral 0D Cs_4PBBr_6 structures with a completely loss of fluorescence. On the other hand, addition of oleic acid induces the transformation of nanocubes into still emitting orthorombic 2D nanoplates, with tunable thickness/lateral size,

according to experimental parameters. The acid/base equilibrium between the two ligands acting as Lewis acid and base respectively, the dynamic between adsorbed and free ligands in solution and the ligand solubility in non-polar solvent are key factors inducing the stabilization/destabilization of the $CsPbBr_3$ structures and morphologies and cannot be eluded for the effective use of these material for technological applications.

Keywords Lead halide perovskite nanocrystals, surface chemistry, ligands equilibria, long term stability

Introduction

Since the first reports on solution phase synthesis [1], all-inorganic cesium lead halide perovskite (CsLHP) nanocrystals (NCs) have shown exceptional photophysical properties, greatly enhanced compared to those of conventional chalcogenides [2-4]. Such excellent optoelectronic properties include a direct band gap tunability over the entire visible spectral range by control of NC size and composition through anion exchange, a large optical absorption cross section, a very bright emission with high photoluminescence (PL) quantum yield (QY), a long carrier diffusion length and a large charge carrier mobility [5]. The outstanding characteristics of CsLHP NCs, accounted by the ionic structure and the high defect tolerance factor [3, 4], are, however, hampered by the stability issues of this class of materials. In fact, the all-inorganic colloidal CsLHP, although less thermal/moisture sensitive than the organic-inorganic counterpart [4, 6], still present limitations in term of stability, thus requiring care and attention in processing and for their integration in devices [7]. In particular, the ionic nature of CsLHP NCs is responsible of their fast deterioration that may result in NC dissolution in solution, further accelerated by their high surface area. As an example, purification procedures and redispersion in solvent of the as synthesized colloidal CsLHP NCs have been reported as crucial steps, able to induce NC destabilization. Solvents as acetone [1], tert-butyl alcohol [1], ethyl acetate [8], and isopropyl alcohol [9] with a relatively low polarity [10] are used as non-solvents

in purification procedures, rather than the generally used protic solvents as methanol and ethanol, presenting a polarity too high to preserve the CsLHP integrity. Accordingly, solvents like anhydrous hexane or toluene, with polarity lower than chloroform, are used to disperse the CsLHP NCs. A key role in the limited stability of the CsLHP NCs has been also accounted to the organic-inorganic interaction between alkyl amine and alkyl carboxylic acid, used as ligands, and the NC surface [11-13]. Irrespectively of the synthetic protocol, that may be based on solution phase hot injection [1, 8, 12, 14-21] or ligand assisted precipitation at room temperature [22-26], alkyl amine and carboxylic acid have shown their potential in regulating the final morphology of the NCs, promoting the selective formation of nanocubes [1, 12, 14], nanoplates (NPLs) [16-18, 21], nanowires (NWs) [8, 20], acting on a acid base equilibrium mechanism [18]. Moreover, alkyl amine and carboxylic acid has been proven essential to determine the surface chemistry of the nanostructures [11, 12]. Indeed, alkyl ammine (mainly oleylamine, Olam) or carboxylic acid (mainly oleic acid, Olac) are reported to behave as Lewis base and acid, respectively, stabilizing the NCs in solution with alkylammonium, forming hydrogen bond with bromide anionic surface sites, and alkyl carboxylate binding the surface cationic sites. However, ligands interaction [11] with the NC surface is labile and caused rapid desorption of the protective ligand layer, for example upon isolation and purification of colloids, affecting the colloidal stability and optical properties [12, 13, 27]. Recently, Krieg F. et al [27] described the improved chemical stability and preserved PL properties of CsLHP NCs prepared by hot injection procedures by replacing alkyl amines and carboxylic acids with zwitterionic ligands, able to coordinate simultaneously the surface cations and anions, thus pointing out the essential role of surface chemistry in CsLHP NC stabilization. However, the use of these bifunctional zwitterionic ligands poses strong limitation to the ability of effectively engineering the morphology of the final nanostructures through the versatile combinations of both alkyl amine and carboxylic acid as ligands. The dynamic binding of the ligands to the NC surface, the acid-base equilibrium between organic acid and base ligands, the low energy formation, which makes the surfactant controlled recrystallization of free ions in solution a viable process at room temperature, all contribute to render

CsLHP materials particularly sensitive to environmental and processing conditions and prone to undergo to structural, morphological and, hence spectroscopic, transformations.

In this perspective, here, we investigate the effect of post-preparative treatments on $CsPbBr_3$ colloidal nanocubes, prepared by hot injection approach. Among the all-inorganic CsLHP, numerous studies focus on $CsPbBr_3$, more stable in terms of photophysical properties under ambient condition than $CsPbI_3$. In fact iodide based NCs, obtained in the cubic phase at high temperature, turn into the photoinactive orthorhombic δ- $CsPbI_3$ phase below 100°C [28]. Nonetheless, a versatile and reversible conversion of 3D $CsPbBr_3$ nanocubes to 0D rhombohedral lead halide deficient non perovskite Cs_4PbBr_6 nanostructures by post-synthetic temperature and chemical treatments with alkyl amine has been recently reported [29-34], pointing out the softness of $CsPbBr_3$ [35, 36].

Here, we report on the systematic investigation of the spectroscopic, morphological and structural properties evolution of as prepared $CsPbBr_3$ nanocubes upon ligand addition (alkyl carboxylic acid or alkyl amine), solvent dilution and ageing experiments. In particular, the post-synthetic treatment with alkyl carboxylic acid or alkyl amine induces a surfactant controlled transformation of 3D nanocubes into 2D NPLs, when Olac is added, and into 1D NWs and 0D Cs_4PbBr_6 crystals, respectively, when Ola) is adjoined at room temperature. The exhaustive investigation shed a new light on NC surface chemistry, ligand dynamic interaction with NC surface and their equilibria in solution. Interestingly, the observed deterioration of $CsPBr_3$ colloidal NCs is mainly ascribed to modification of ligand equilibria, also driven by the ionic structure of CsLHP and low energy formation, finally resulting in severe structural and morphological transformations and, consequently, changes in the optoelectronic properties.

1. Experimental section.

Materials. $PbBr_2$ (98%), octadecene (ODE, 90%), oleic acid (Olac, 90%), oleylamine (Olam, 70%), octylamine (Octa, 99%), Cs_2CO_3 (99.9%), %), hexane (anhydrous 95%), were purchased from Sigma-Aldrich and used without any further purification.

Solution-based synthesis of colloidal $CsPbBr_3$ NCs. The synthesis of $CsPbBr_3$ NCs was carried out according to the procedure reported by Protesescu *et al*. with minor modifications [1]. A mixture of 0.4 mmol of $PbBr_2$, 10 mL of ODE (40m M), 3.0 mmol of Olac (0.3 M) and 3.0 mmol of fresh Olam (0.3 M) was prepared in a three necked flask and put under vacuum at 80 ° C for 1h and at 150°C under nitrogen flux for 30 min. In a second three-necked flask the cesium precursor was prepared by dispersing 0.4 mmol of Cs_2CO_3 in 5mL of ODE ($[Cs^+]$ =80 mM) with 2.5 mmol of Olac (0.5 mM). The mixture, firstly put under vacuum at 100 ° C for 1h, was subsequently heated to 150 ° C under N_2 atmosphere to allow the complete decomposition of Cs_2CO_3 and formation of Cs-oleate (pale yellow solution). 0.8 ml of Cs-Oleate (0.06 mmol) was injected in the lead and bromine mixture at 140 ° C suddenly cooled down at room temperature by immersion in ice bath. At this stage, the reaction mixture turns into an intense yellow-green color. The NCs were collected by centrifugation at 9000 rpm for 90min at 10 ° C without addiction of any non-solvent and redispersed in 6mL of anhydrous hexane. The concentration of this solution expressed in terms of Pb content resulted 60 mM.

Post-synthetic ligand treatments were carried out by adding Olac ranging from 25µL/mL (0.075M) to 50µL/mL (0.15 M) or Olam, ranging from 25µL/mL(0.075M) to 50 µL/mL (0.15 M), to the as synthesized $CsPbBr_3$ colloidal solution. The sample was then centrifuged at 1000rpm for 10 minutes at room temperature and the supernatant was recovered for further characterization.

Characterization techniques. For transmission electron microscopy (TEM) analysis, samples were prepared by dipping a carbon-coated copper grid into the NC solution at 1:100 dilution with anhydrous hexane. TEM imaging was carried out using a JEOL JEM1011 microscope, operating at an accelerating voltage of 100 kV and equipped with a W electron source anda CCD high resolution camera. Statistical analysis of the size (NC average size and size distribution) of the samples was performed by using of a freeware image analysis program. The percentage relative standard deviation (σ%) was calculated for each sample, providing information on the NP size distribution. Its value is based on the distribution of size compared to the average value and is expressed as a percentage.

SEM analyses were carried out by mean of field emission scanning electron microscopy (FE-SEM) Zeiss Sigma operating in the range 0.5–20 kV and equipped with an in lens secondary electron detector. FE-SEM samples were prepared by spin coating the NC solution at 1000 and 2000 rpm for 30s, with a subsequent thermal treatment at 40°C for 5 minutes, to let the solvent to completely evaporate and the spin coated film to dry. The substrates were then placed onto stainless-steel sample holders for SEM measurements.

UV-Vis absorption spectra were recorded with a Cary 5000 (Varian) UV/Vis/NIR spectrophotometer by solvent diluting the crude solution 1:100.

All fluorescence measurements were performed at room temperature on solid film: 100 μL of NC solution were spin coated onto a quartz 1x1cm^2 slide (800rpm for 30s), and then thermally treated at 40°C for 5 minutes. Fluorescence spectra were recorded by using a Fluorolog 3 spectrofluorimeter (HORIBA Jobin-Yvon), equipped with double grating excitation and emission monochromators. Time resolved photoluminescence (TRPL) measurements were performed by Time-Correlated Single Photon Counting (TCSPC) technique, with a FluoroHub (HORIBA Jobin-Yvon). The samples were excited at 375 nm by means of a picosecond laser diode (NanoLED 375L) with a pulse length of 80 ps at a 1 MHz repetition rate. The PL signals were dispersed by a double grating monochromator and detected by a picosecond photon counter (TBX ps Photon Detection Module, HORIBA Jobin-Yvon). The temporal resolution of the experimental set up was ~200 ps. The values of the absolute quantum yield and 1931 CIE colour point measurements were obtained by means of a ‘‘Quanta-phi’’ integrating sphere coated with Spectralons® and mounted in the optical path of the spectrofluorometer, using as an excitation source a 450 W xenon lamp coupled with a double-grating monochromator.

Grazing Incidence Wide Angle Scattering (GIWAXS) patterns were collected at 2° incidence angle with a Rigaku Fr-E+ rotating anode microsource (CuKα radiation) coupled to a SAXS/WAXS camera.[37] An image plate with 100 μm pixel size was used as a detector, placed at 87mm distance from the sample. Patterns were calibrated by using Ag Behenate standard powder as a reference.

Coupled sample-detector X-Ray Diffraction (θ/2θ XRD) scans were collected by a Bruker D8 Discover (CuK_α radiation), equipped with a Göbel mirror on the primary beam and a scintillation point detector. Samples for analysis were prepared by drop casting the colloidal solutions on silicon substrates and let evaporate in open air.

2. Results

Synthesis and characterization of $CsPbBr_3$ nanocubes. $CsPbBr_3$ NCs are synthesized by using the hot injection approach reported by Protesescu *et al* [1]: Cs-oleate precursor (0.06 mmol) is injected at 140°C in an octadecene solution containing $PbBr_2$ (0.4 mmol), previously dissolved in the presence of an equimolar combination of Olac/Olam (0.3 M/0.3M). TEM characterization of the samples (Figure 1a, sample diluted at nearly 0.7 mM Pb concentration), recovered from the reaction mixture by centrifugation and without addition of a non-solvent, shows the presence of square-shaped structures, quite homogenous in size, with a lateral size of 8 nm and size distribution σ% = 17 % (Figure 1b). Smaller nanocubes, nearly 4 nm in edge length, are collected at higher centrifugation rate from the supernatant (ESI, Figure S1e).

The poor solubility of lead halide precursor in octadecene [14] can be effectively improved by the combined use of both Olam and Olac in the reaction mixture. The binary mixture of alkyl amine and alkyl carboxylic acid ligands does not only serve for precursor solvation, cation coordination and ligand stabilization of the nanostructures, but, according to recent findings, it is involved in the acid-base equilibrium and formation of $Olac^-Olam^+$ [14]. The concentration of ligands and their molar ratio result decisive, along with the control of temperature, for the final CsLHP nanostructure size, shape and phase.

Notably, 140°C is usually reported [14, 37] as a threshold temperature between the high yield formation of nanocubes (T > 140°C) and of NPLs (T < 140°C). However, the equimolar (0.3 M/0.3M) concentration of Olam and Olac [14] used here in the synthesis (Figure 1a,) results mainly in nanocubes with a negligible fraction of NPLs.

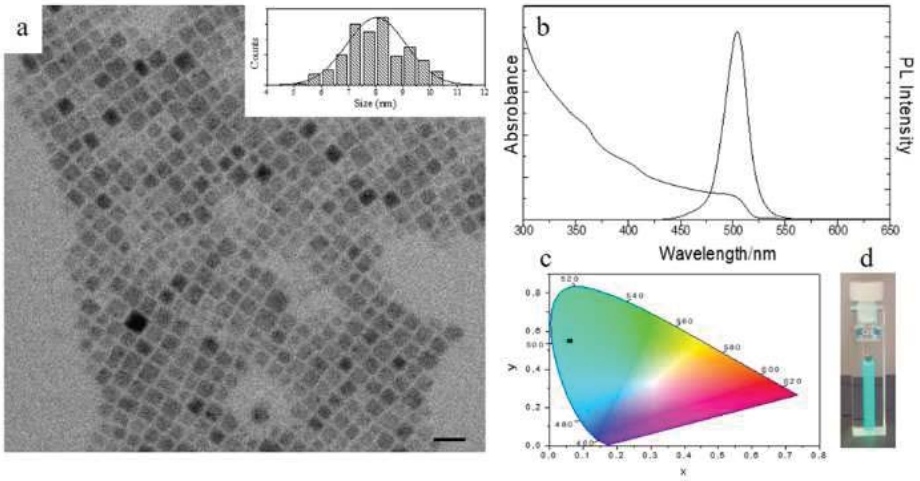

Figure 1 Morphological and spectroscopic characterization of $CsPbBr_3$ NCs. TEM micrograph (a, scale bar 20 nm) and statistical analysis of the NC size (inset, number of counted NCs = 250). UV-Vis absorption spectrum in solution and fluorescence (λex = 375nm) spectrum of NC thin film on quartz prepared by spin coating the NC solution (b) along with the position in the CIE 1931 diagram colour point x = 0.06 y = 0.55 (c). Picture of NC colloidal solution cuvette under illumination with a UV lamp at 365 nm (d).

The UV-Vis absorption spectrum of the as prepared sample (dilution nearly at 0.6 mM Pb concentration, Figure 1b) shows the typical profile of colloidal $CsPbBr_3$ semiconductor nanocubes, characterized by a broad exciton absorption peak at nearly 500 nm [1]. The PL spectrum of $CsPbBr_3$ NC thin film, prepared by spin coating the colloidal solution (7 mM in Pb) on a quartz slide, shows a narrow and intense emission band (full width at half maximum FWHM of 130 meV) centered at 505 nm (2.45 eV). The emission band can be associated to the bulk band gap of $CsPbBr_3$ [38] with a value of the absolute QY value of nearly 75%. The PL characterization in thin film has been purposely carried out since transformation of the as prepared nanocubes upon dilution is observed [38]. Indeed, at dilution needed for PL measurements in solution (down to 0.08 mM Pb, in order to avoid self-absorption phenomena due to the high extinction coefficient of CsLHP NCs $\varepsilon = 10^6$ L mol^{-1} cm^{-1}) [39], the as synthesized 8 nm sized $CsPbBr_3$ NCs turn into very small nanocubes (Figure 2a), with reduced edge length down to 3nm, and anisotropic 2D NPLs structures. The coexistence of small NCs and NPLs shown by TEM is also supported by PL characterization (Figure 2c, red line). The emission spectrum shows a main band blue shifted to 483 nm (2.57 eV) with a FWHM (150 meV), ascribed to

NPLs with a broad distribution in thickness and lateral size, and an additional weak PL contribution at higher energy (2.9 eV) attributed to NCs. In the meanwhile, the emission dramatically decreases and the PL QY drops down to 30% after dilution, probably due to non-radiative recombination pathways in very small nanostructures and also to the reduced number of emitting nanostructures contributing to the PL [40].

In addition to the dramatic size and shape evolution induced in as prepared $CsPbBr_3$ nanocubes upon dilution, also ageing brings morphological transformation of the nanocubes. Under prolonged (longer than one month) air/moisture and light exposure, the TEM grid of as prepared $CsPbBr_3$ nanocubes shows the formation of polydispersed larger nanostructures (Figure 2b), highlighting a limited stability in time of the original nanocubes even on solid phase.

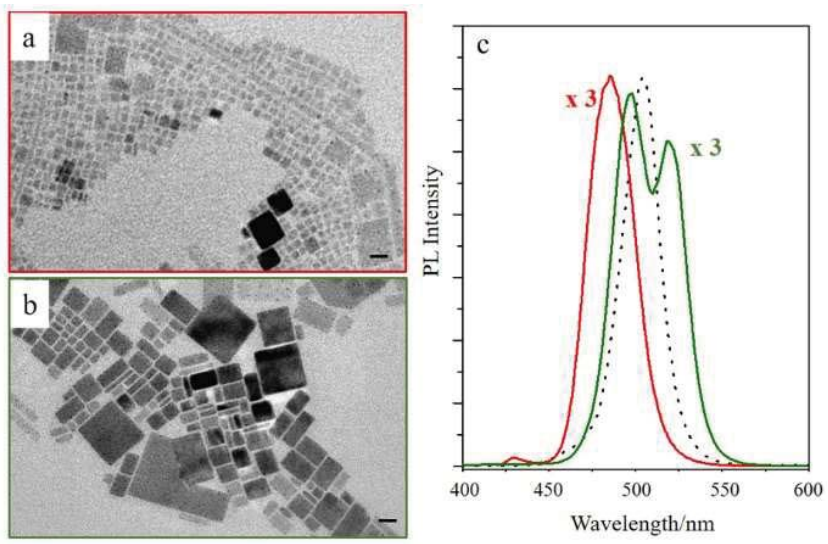

Figure 2 (a,b) TEM micrographs (scale bar 20 nm).and (c) PL spectra (excitation wavelength at 375 nm) of colloidal $CsPbBr_3$ nanocubes just after dilution with hexane at 0.08M Pb concentration (a panel, and red line in c panel) and after ageing the dispersion for a month (b panel and green line in c panel). PL spectrum of spin coated as synthesized undiluted colloidal nanocubes solution on quartz slide (c, dashed line).

This change in morphology is reflected in the PL spectrum, recorded in thin film of NC solution exposed to air. The spectrum presents two contributions (Figure 2c green line) that can be safely assigned based on the TEM characterization (Figure 2b). Namely, the band centered at 505 nm can be ascribed to residual 8 nm-sized nanocubes and the band centered at 519 nm can be attributed to

the larger nanostructures, either nanocubes or NPLs with lateral size and thickness up to tens of nanometer. Upon ageing, progressive PL quenching occurs with a decrease of the PL QY down to 52% after one month.

Room temperature ligand induced transformation from 3D nanocubes to 2D nanostructures: morphologic and spectroscopic characterization. 3D $CsPbBr_3$ nanocubes transform their structure and spectroscopic properties upon treatment with Olam in solution [14, 29-34]. Several groups [14, 29-34, 41] have claimed the transition of 3D $CsPbBr_3$ nanocubes into zero dimensional 0D Cs_4PbBr_6 rhombohedral nanostructures that crystallize as a white powders, upon treatment with Olam in solution. Here, we prove that the concentration of Olam is critical for directing the final morphology, structure and hence spectroscopic properties.

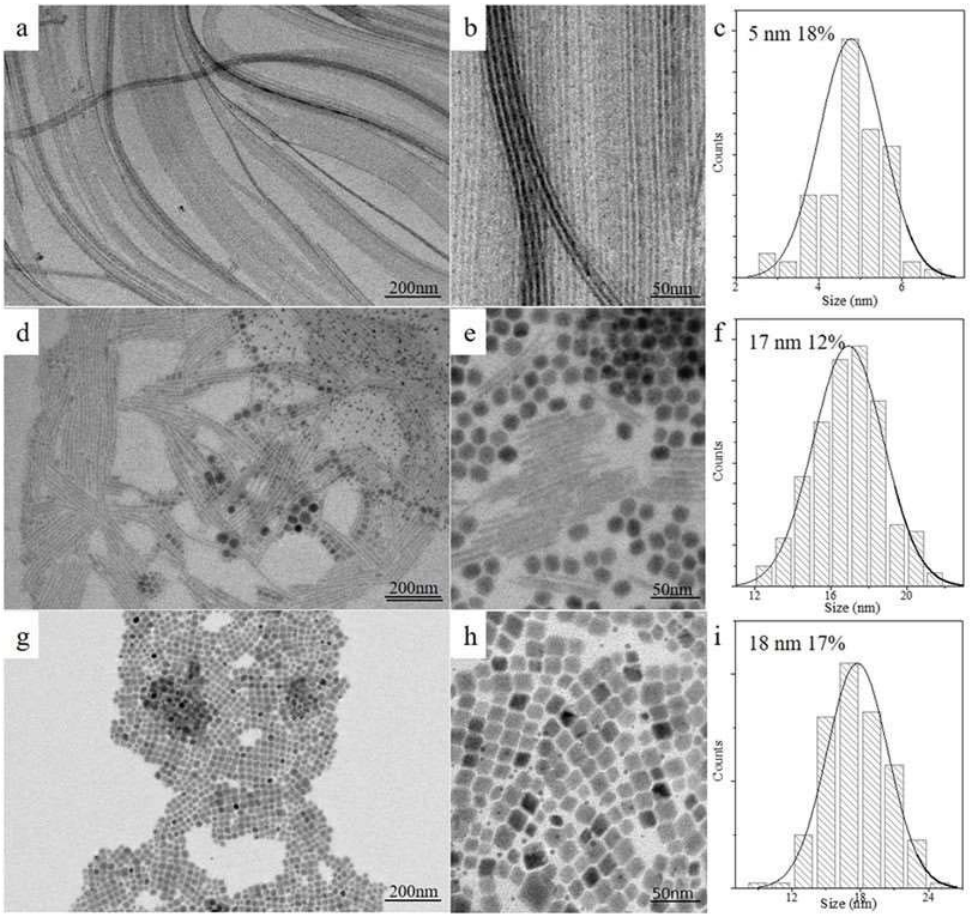

Figure 3. TEM micrographs (a, b, d, e, g, h) of pristine 3D $CsPbBr_3$ upon addition of (a-b) 0.075mmol/mL, (d-e) 0.10 mmol/mL, (g-h) 0.15 mmol/mL of fresh oleyl amine, resulting in Olam 75, Olam 100 and Olam 150 sample, respectively. Size distribution of nanowire width (c) in Olam

75, of spherical nanoparticles diameter in Olam 100 (f) and of lateral size of rhombohedral shaped nanostructures in Olam 150 (i) samples.

In particular, post synthetic addition of 0.075 mmol/mL of Olam to the solution (NC sample named "Olam 75") induces the transformation of the freshly prepared 3D nanocubes into nanostructures similar to nanowires (NWs) over few micrometers long (Figure 3a-c) and 5 nm width (σ%= 18%) along with a small residual fraction of nanocubes. Such NWs, to the best of our knowledge, have not been isolated, so far, by using such a post-synthetic colloidal approach,

Notably, after addition of 0.10 mmol/mL of Olam (Figure 3d-f, NC sample named "Olam 100") the 3D nanocubes turn into NWs tens of nanometers long with nearly 5 nm width together with abundant large spherical nanoparticles of nearly 17 nm in diameter, quite homogenous in size (σ%= 12%). Further, addition of Olam at a concentration > 0.15 M (Figure 3g-I, NC sample named "Olam 150") brings to the formation of rhombohedral shaped nanostructures with a lateral size of nearly 18 nm (σ%= 17%) and the separation of a white precipitate. However, the NWs, in Olam 75 sample, although retaining their size and shape regime for more than a weak, slowly turn into larger rhombohedral structures, similar to those reported in Figure 3g-i, in approximately three weeks (See ESI S2a,c), thus allowing to infer that these nanostructures represent a sort of metastable intermediate. Similar findings have been achieved by adding shorter alkyl chain amine such as octylamine (See ESI Figure S3), indicating that the shape transformation of 3D nanocubes can be ascribed to the amine functional groups. While the absorption spectrum (Figure 5a orange line) of Olam 75 sample does not show appreciable changes in exciton position compared to the as synthesized nanocubes (Figure 5a black line), PL characterization results much more sensitive to the shape transformation. Indeed, the absorption spectrum of Olam 75 sample can be ascribed to residual nanocubes, still detected in the sample by the TEM analysis, whose absorption line profile hides that of the NWs, expected to have a spectroscopic signature with an exciton absorption blue shifted due to quantum confinement of NW width (Bohr diameter for $CsPbBr_3$ is 7 nm) [39]. Conversely, the PL characterization (Figure 5b, orange line) shows a broaden and almost quenched spectrum, different from that of the as prepared

nanocubes (Figure 5b black line). The poorly intense emission band centered at 505 nm can be ascribed to the very few residual nanocubes, while the prominent shoulder at higher energy is originated by the emission of thin NWs that contribute to the PL at lower wavelength, due to quantum confinement. Meanwhile the absolute PLQY decreases down to 4% due to the low amount of residual nanocubes and to the trap states in thinnest NWs [42]. Additional increase of the Olam amount (Olam 150 sample) results in a completely loss of fluorescence and in a dramatic change of the absorbance spectrum (Figure 5a, wine line). The characteristic exciton absorption of the $CsPbBr_3$ turns into a weak signal blue shifted at 430 nm, due to the presence of degraded residual $CsPbBr_3$ very small nanocubes,[16] with an intense band at 311 nm, ascribed to the individual $PbBr_6^{4-}$ clusters[14, 32] of the 0D Cs_4PbBr_6, forming at this Olam concentration, as demonstrated by structural investigation (See following section).

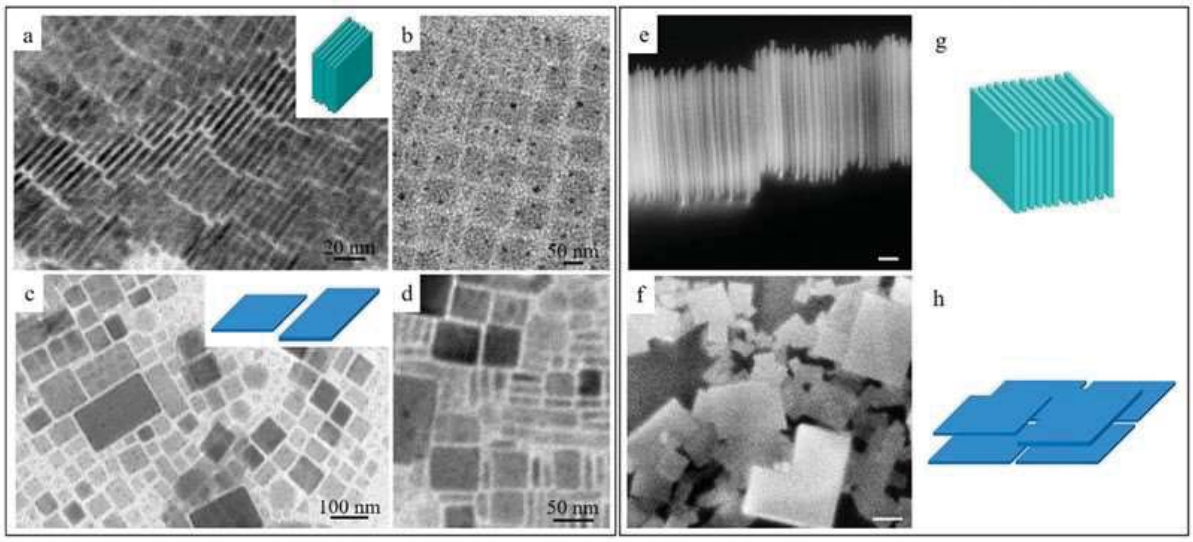

Figure 4 TEM micrographs (a-d) and SEM images (e, f) of oleic acid (Olac) treated $CsPbBr_3$ nanocubes transforming into nanoplates. TEM images of samples upon addition of 0.075mmol/mL (a, b, Olac 75) and 0.15 mmol/mL (c, d, Olac 150) of Olac to the as prepared $CsPbBr_3$ nanocubes (see Figure 1a). SEM images (e, f, scale bar 100 nm) and schematic sketches (g, h) of stacked (e, g) and lateral-oriented attached (f, h) nanoplates prepared at 0.15mmol/mL Olac-treatment. Using a spin coating deposition at low speed (1000 rpm e) nanoplates arrange by edge on the substrate facing each other in stacked structures with a long range order, while at high spin speed (2000 rpm, f), nanoplates preferentially lie face on the substrate.

While alkylamine promotes the formation of 1D and lead halide depleted 0D nanostructures, addition of Olac to the solution of the as prepared 3D $CsPbBr_3$ nanocubes (Figure 1a) results in the formation

of 2D anisotropic nanoplates (Figure 4), irrespectively from the amount of Olac added. In particular, with 0.075mmol/mL of Olac, the pristine nanostructures evolve into 4 nm thick NPLs with a lateral size up to nearly 40 nm (NC sampled named "Olac 75"), sitting with the edge on the TEM grid (Figure 4a-b) in a typical close packed face-to face organization [37], although residual 8 nm sized nanocubes can be still observed by TEM characterization. At higher concentration of Olac (0.15 mmol/mL, NC sample named "Olac 150"), larger platelets are obtained, with lateral size of few hundreds of nanometers (Figure 4c-d), which preferentially assemble face on the TEM grid. Upon ageing, the small NPLs, that remain stable for more than one week, turn into widely polydisperse NPLs with micrometer sized edge (See ESI 2b, d).

Absorption spectrum of Olac 75 sample (Figure 5, cyan line) shows an exciton transition signal blue shifted to 485 nm, narrower and more pronounced with respect to that of the as prepared 3D nanocubes (500 nm), attributed to NPL structures (Figure 5a cyan line) [17, 18, 21, 39, 43, 44]. Remarkably, the thickness of the NPLs of 4 nm, approximately corresponding to a three perovskite multilayered structure, is expected to be still in quantum confinement regime [39]. The emission spectrum (Figure 5b cyan line) is characterized by a main band at 503 nm, ascribable to residual nanocubes, and a blue shifted shoulder at nearly 480 nm attributed to NPLs, with thickness smaller than the Bohr diameter [18].

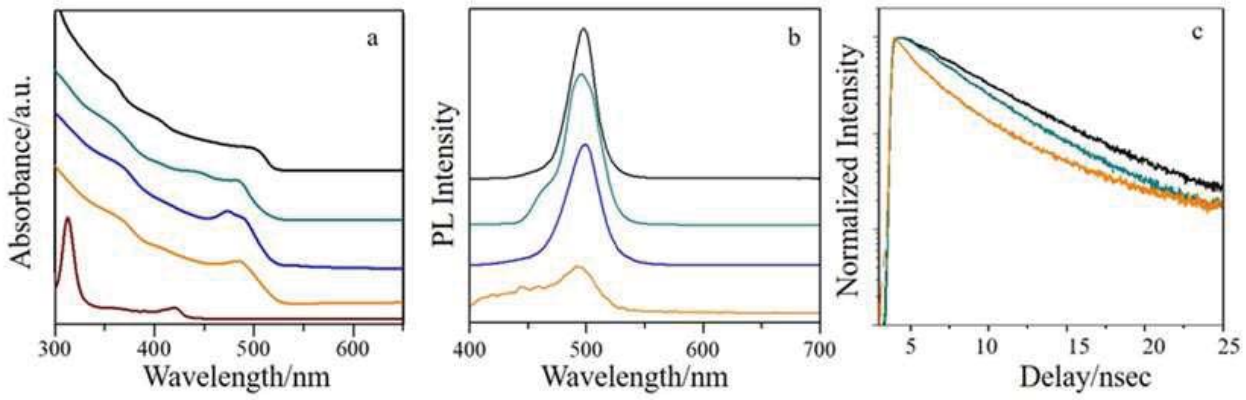

Figure 5 UV-vis absorbance (a), emission (b) spectra and time resolved PL decay (c) of as prepared (black line), oleyl amine (Olam 75, orange line, Olam 150 wine line) and oleic acid (Olac 75 cyan line and Olac 150 blue line) treated $CsPbBr_3$ samples. The traces are vertically shifted for sake of clarity.

Spectra of Olac 150 sample, obtained upon addition of 0.15 mmol/mL of Olac, shows an exciton absorption signal (Figure 5a blue line) and PL band (Figure 5b blue line), centered at 495 nm and 505 nm, respectively, consistent with the evolution towards larger NPLs, as confirmed by the TEM characterization. The formation of NPLs turns in an only partial quenching of the emission QY (PLQY 56%) with respect to the as prepared sample.

Time-Correlated Single Photon Counting (TCSPC) measurements (Figure 5c) of the as synthesized nanocubes (Figure 5c black line), Olam 75 (Figure 5c, orange line) and Olac 75 samples (Figure 5c, cyan line), consisting in NWs and NPLs, respectively, deposited in thin films, result well fitted by a three exponential function and the average lifetimes, reported in the ESI (Table S1), are in line with previous findings [16, 23, 39]. However, a significant difference in the decays of the different nanostructures is evident, even better highlighted on a double logarithmic scale (Figure S6) in the first few nanoseconds after the excitation. Indeed, the decay of both nanocubes and NPLs shows a faint rise time, not evinced for NWs. This can be ascribed to the large distribution in size of both nanocubes and NPLs, that induces a mechanism of energy transfer among NCs, more pronounced in the samples deposited as thin film, where the nanostructures result in close proximity [45]. The emission from nano-objects of smaller size, properly excited at high energy, can be absorbed rapidly by larger nanostructures, resulting in an increase in the excited population with a delay that originates the rise time phenomenon. In the case of NWs such an effect is not observed, due to the strong PL quenching and the different packing arrangement.

Room temperature ligand induced transformation from 3D nanocubes to 1D and 2D nanostructures: structural characterization. The results of the systematic structural investigation of the as prepared, aged and post-synthesis treated (with Olam or Olac, at different concentration) samples is reported in Figure 6 and Figure 7 (see also ESI Figure S4-S5). It is worth to note that the XRD patterns of each samples have been recorded from films drop cast on silicon substrate, each XRD profile resulting from all the nanostructures composing the sample.

The XRD pattern profile of the as prepared sample, reported in Figures 6c (solid line), well fitted (see ESI Figure S4 black line) using a cubic structure model, confirms the perovskite lattice structure with $CsPbBr_3$ stoichiometry, with a 5.871 Å unit cell size. The 8 nm NC size calculated along the [100] direction is in agreement with the average lateral size of the nanocubes resulting from TEM characterization. However, the significant signal broadening, due to nanocube small size, does not allow to univocally correlating the experimental diffractogram to a specific crystalline phase. Peak positions, indeed, fit with cubic lattice (ICDD # 01-072-7930, Figure 6a), monocline (ICDD 00-018-0364, Figure 6b), tetragonal (ICDD #01-074-6645 Figure 6g) and orthorhombic (ICDD #01-072-7929, Figure 6h) reference patterns.

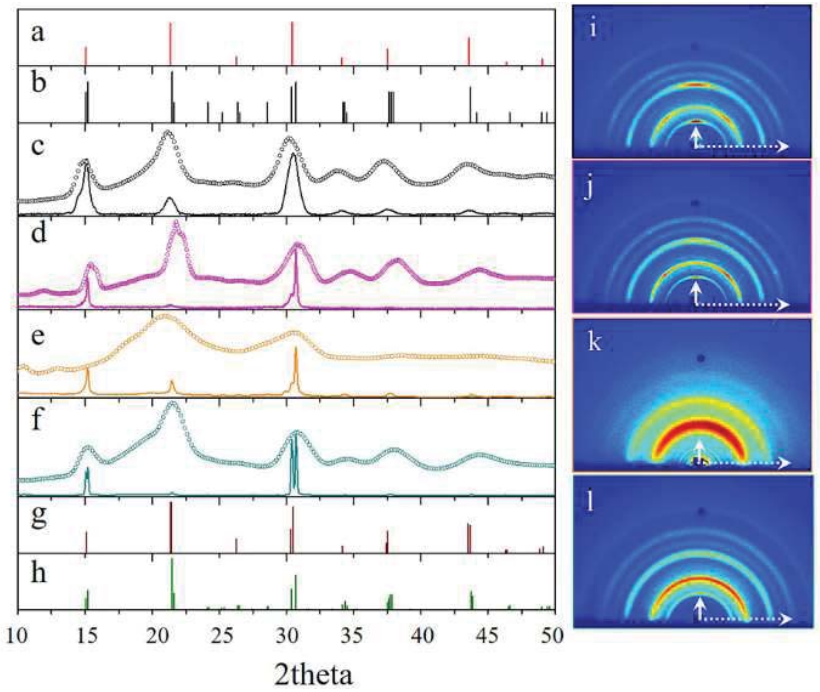

Figure 6. XRD patterns collected in coupled sample-detector (θ/2θ) scan mode (c-f, solid line), and in grazing incidence (GIWAXS) geometry with 2 degree incidence angle: radial profile (c-f, circle symbol) and 2D maps (i-l) of as prepared (c,i), one month aged (d, j), 0.075 mmol/mL oleyl amine, (e, k, Olam 75) and 0.075 mmol/mL oleic acid (f, l Olac 75) treated samples. Reference XRD patterns for cubic (ICDD # 01-072-7930, a) monocline (ICDD 00-018-0364, b), tetragonal (ICDD #01-074-6645, g) and orthorhombic (ICDD #01-072-7929, h).

Therefore, here we exploit a combined evaluation of θ/2θ XRD patterns and GIWAXS radial profiles azimuthally averaged and also taken along specific directions (typically in and out of the sample plane, see ESI S5). Peak position, broadening and intensity have been compared with reference patterns in order to unveil the crystalline phases of the as prepared nanocubes (and similarly for the

aged and ligand treated samples). θ/2θ XRD geometry provides a higher accuracy in terms of peak position and lower instrumental broadening, though the relative intensity of reflections can be affected by NC preferred orientation, possibly resulting in the damping of some reflections compared to reference powder diffraction patterns. On the other hand, the collection of GIWAXS data on a 2D detector allows to readily recognize the presence of preferred orientations; moreover, the profile obtained by fully integrating the scattering intensity along the azimuth is much less affected by preferred orientations, and thus can be directly compared to the diffraction pattern expected for a polycrystalline powder. In particular, the combined evaluation of the 2θ = 30.5°/15.1° intensity ratio from the θ/2θ XRD profile, and the 30.5°/21.3°one from the azimuthally averaged GIWAXS profile, allow to discriminate among the variety of crystalline structures corresponding to the same perovskite ABX_3 stoichiometry. The 30.5°/21.3° intensity ratio was evaluated from the azimuthally averaged GIWAXS profile, since preferred orientation of the NCs, which is evident from the GIWAXS 2D map in Figure 5i, produces a clear damping of the 21.3° peak in the θ/2θ XRD pattern, compared to the reference pattern. Conversely, the θ/2θ XRD pattern provides the correct relative intensity for the 15.1° and 30.5° peaks, which are the first and second diffraction order (i.e. both peaks come from the same lattice planes) for cubic, monocline, orthorhombic crystalline phases.

The 30.5°/15.1° intensity ratio of nearly 1.1 (Figure 6c, solid line) for the as prepared sample is more characteristic of the monocline (30.5°/15.1° nearly 1, ICDD 00-018-0364) and cubic (30.5°/15.1° nearly 1.3, JCPDS #18-0464) phase rather than matching the orthorhombic (30.5°/15.1° nearly 1.8, ICDD #01-072-7929) ones. These values are also smaller than those expected for the tetragonal phase (30.5°/15.1° intensity ratio nearly 3.3, ICDD #01-074-6645) for which the peaks at 15.1° and 30.5° correspond to the 100 and 002/200 reflections, respectively. On the other hand, cubic and monocline phases cannot be discriminated based on the 30.5°/21.3° intensity ratio, as they feature similar values in the integrated GIWAXS profiles. A complete phase transformation of the as prepared nanostructures to orthorhombic is demonstrated upon ageing experiments. A30.5°/15.1° intensity

ratio of nearly 1.9 (Figure 6d solid line) and a 30.5°/21.3°intensity ratio of nearly 0.6 (Figure 6d circle symbols) resulted for the aged sample, better matching the expected values for the orthorhombic phase (1.8 and 0.8, respectively). The 30.5° and 15.1° peaks clearly split resulting in a doublet, with a net increase in intensity of the peak at larger 2θ for each doublet, indicating a domain size increase and a morphological evolution towards highly anisotropic shape in agreement with TEM characterization (See Figure 2b). The two peaks at 15.1° and 30.5° can be thus assigned to 002/110 and 004/220 reflections and the 21.3° one to the 112/020/200 reflection of the orthorhombic phase (ICDD #01-072-7929), respectively. Since the 110 (220) peak results sharper, while the 002 (004) appears as a low intense shoulder, the [110] can be assumed as the anisotropic growth direction.

Shape and phase ligand assisted transformation. Olam addition. The θ/2θ XRD (Figure 6e, solid line) and GIWAXS integrated profile (Figure 6e, circle symbol) for Olam 75 sample are different from each other, thus suggesting that they account for different species. The θ/2θ XRD pattern (Figure 6e solid line) is quite similar to that of the aged sample, therefore accounting for residual $CsPbBr_3$ nanocubes. On the other hand, the GIWAXS characterization (Figure 6e circle symbol, and Figure 6k 2D map), reveals an overall peak broadening in the radial profile and disappearance of the 15.1° peak, which indicate a decrease of the nanostructure domain size and the loss of the pristine phase, respectively. Notably, the suppression of the peak at 15.1° could be compatible with a transition to the tetragonal phase, where the 15.1° and 30.5° peaks are no more different diffraction orders form the same lattice planes, but independent reflections: 100 and 002/200, respectively. Therefore, the 100/200 reflections can be assumed to damp due to the decrease of the crystalline domain in the *a*,*b* plane, whereas the 002 reflection still features a significant contribution around 30.3°, compatible with a tetragonal nanostructure anisotropically elongated along the *c* axis. Transformation of $CsPbBr_3$ stoichiometry into Cs_4PbBr_6 phase, as reported in literature to be induced by alkyl amine addition to the as prepared nanocubes and as suggested in the previously reported morphological and spectroscopic characterization, is confirmed by the XRD (θ/2θ) pattern (Figure 7b) of the Olam 150

sample, featuring sharp peaks superimposed on a background ascribed to Olam, that well agrees with Cs_4PbBr_6.

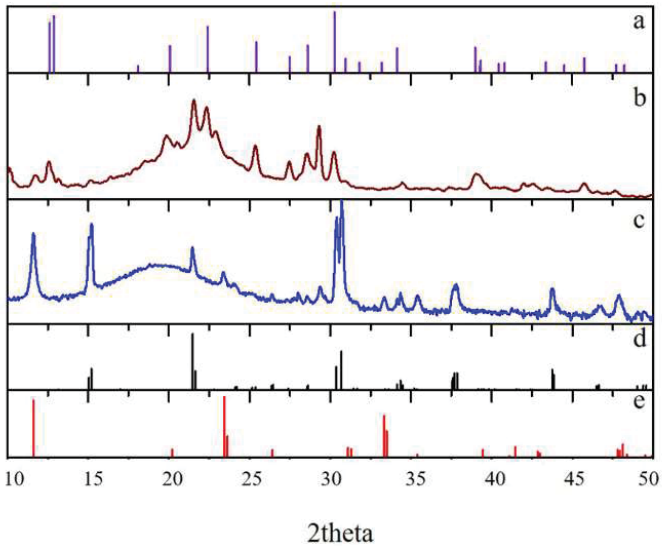

Figure 7 XRD reference pattern of rhombohedral Cs_4PbBr_6 ICSD #025124 (a), orthorhombic $CsPbBr_3$ ICDD #01-072-7929 (d) and Cs_3O ICSD # 015695 (e). XRD (θ/2θ) characterization of Olam 150 (b) and Olac 150 (c) samples.

Shape and phase ligand assisted transformation. Olac addition. XRD (θ/2θ) patterns (Figure 6f and Figure 7c) demonstrate that irrespectively from the amount of Olac added (Olac 75 and Olac 150 samples), NPLs have an orthorhombic phase. The sharp 15.1° and 30.5° reflections clearly split into two contributions, with an intensity ratio (2.2) closely matching the value expected for the 002(110)/004(220) orthorhombic reflections confirmed the increase in the size domain, i.e. lateral size, as evidenced in TEM analysis (Figure 4). Such sharp peaks indicate the preferential edge-on orientation and the crystallographic directions of the growth plane of the NPLs, which can reach up to hundreds nm size, as shown in Figure 4a-d. Accordingly, the diffraction peak at 21.3° (112/020/200) remains broad and almost quenched (Figure 6f, solid line), being related to a crystallographic direction oriented across the small NPLs thickness.

3. Discussion

While the exceptional optoelectronic properties of colloidal $CsPbBr_3$ nanostructures have been already widely recognized, still their limited stability due to the ionic nature, the weak interaction of

lead halide interlayers and the labile ligand/NC surface interaction [11] remain critical issues for their application in devices. Here, the role of surface treatment/post synthetic functionalization procedures in the stabilty of the final $CsPbBr_3$ nanostructures is rationalized [14, 29-34, 38, 43] and the mechanisms driving the size/shape transformation under different processing condition are depicted. Focusing on the structure and surface chemistry of $CsPbBr_3$ NCs, it is generally accepted that the as prepared colloidal $CsPbBr_3$ nanocubes can be considered as an inorganic 3D network where the octahedral $[PbBr_6]^{4-}$ share each Br^- anion, at the corner, with the cesium occupying the cuboctahedral cavity and Olam and Olac adsorbed at the surface by hydrogen bonds (H••••Br) or coordinating (transition) metal, in equilibrium with free ligands in solution [11, 15]. In particular, oleylammonium bromide and oleate stabilize the $CsPbBr_3$ structure. The precise phase determination of all-inorganic nanosized colloidal $CsPbBr_3$ NCs has represented a critical issue due to several possible stoichiometries and crystal lattice distortions, thermodynamically favored at room temperature that lead to different crystalline phases featuring similar diffraction patterns [3, 16]. In addition, the nanosized regime, with its characteristic broadening of diffraction peaks, render phase discrimination even more difficult [3]. Though $CsPbBr_3$ NCs with a cubic perovskite structure are expected at high temperature, recent report [3] pointed out that the orthorhombic phase represents the thermodynamically stable structure at room temperature. However, the structural characterization here reported highlights that monocline or cubic phase, rather than orthorhombic XRD pattern, describes the structure of the as synthesized nanocubes. Prolonged moisture, light and air exposure finally induce morphological and structural change, with 8 nm-sized nanocubes transforming into the large (lateral size >100 nm) anisotropic nanostructures having a clear orthorhombic phase, thus confirming the longer structural stability of this crystalline phase over cubic and monocline under ambient condition.

The complete characterization has proven that transformation of as prepared nanocubes can be pushed further and controlled, by purposely shifting the equilibrium between the absorbed and free ligands

and the acid-base equilibrium between the alkyl carboxylic acid (an organic acid) and the alkyl amine (an organic base).

Interestingly upon dilution with an anhydrous organic solvent (hexane, toluene), the 8 nm sized $CsPbBr_3$ nanocubes evolve towards thinner 2D NPLs, with increased lateral size, and smaller 3D nanostructures, thus corroborating the changes in the optical properties, including the PL blue shift, the multiple emission bands, and the increase in the FWHM. The solubility of the alkyl amine and alkyl carboxylic acid ligands in the non-polar solvent used for dilution can be considered a decisive factor for the comprehension of the phenomena responsible for the observed shape/size change. Ligand molecule desorption, induced at increasing dilution due to the ligand solubility in the non-polar solvent, alters the equilibrium between adsorbed and free ligands and may favor aggregation. Conversely, dissolved cationic ligands (such as alkyl ammonium) present in solution upon protonation by organic acid (such as alkyl carboxylic acid) can easily exchange Cs^+ at the nanostructure surface or can insert themselves between the weakly interacting lead halide interlayers, inducing solvent diffusion inside the NC structures (the so called osmotic swelling) that finally results in structural changes and fragmentation [43]. On the other hand, it is not surprising that, since the low energy formation of $CsPbBr_3$ do not require thermal activation to achieve high crystalline nanostructures, surfactant-controlled co-precipitation of ions in solution, which proceeds with fast kinetics even at room temperature, results in anisotropic growth of the nanocubes and formation of NPLs with increased lateral size [46].

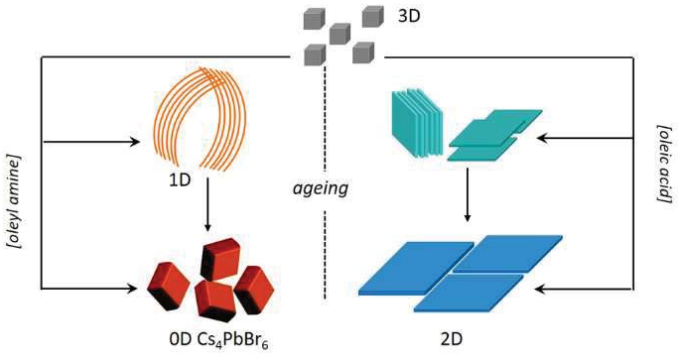

Scheme 1 Shape transformation of $CsPbBr_3$ nanocubes upon ligand addition.Scheme of the morphological transformation of the as prepared 3D $CsPbBr_3$ nanocubes to lower dimensional cesium lead halide derivatives.

Similarly, dynamics between ligands in solution and adsorbed on NC surface is altered due to ambient exposure during ageing of the as prepared nanocubes. Moisture (and light) can cause rapid desorption of the protective ligand shell resulting in an averaged increase of the nanostructure size and surfactants-assisted formation of 2D anisotropic structures.

However, the post-synthesis addition of fresh ligands (Olam and Olac, see Scheme 1) has been found to have the strongest effect on the control of $CsPbBr_3$ shape (Figure 3-4) and to be decisive in driving the structural transformation (Figure 6-7), ultimately resulting in the modification of photophysical properties (see Figure 5 and ESI Figure S6).

The addition of alkyl amine has been widely reported to induce the transformation of the 3D $CsPbBr_3$ nanocubes into 0D Cs_4PbBr_6 [14, 29-34, 41], with each $[PbBr_6]^{4-}$ surrounded by 8 Cs^+ ions and the Br^- no longer shared between the $[PbBr_6]^{4-}$. The emission properties of Cs_4PbBr_6 NCs have been longer debated and are still unclear, as both intense emission properties and a complete quenching of the photoluminescence have been reported. Here, photo-inactive Cs_4PbBr_6 NCs form starting from nanocubes solution upon addition of high amount of Olam (>0.15mmol/mL, Olam 150 sample). The strong binding affinity of Olam, in particular, and alkylamine, in general, for the Pb^{2+} ions can be considered the driving force that, through lead bromide depletion, causes distortion of the 3D $CsPbBr_3$, ending up into a completely different phase based on 0D Cs_4PbBr_6 [29].

However, in this work, we have been able to isolate an intermediate metastable 1D structures (Olam 75 sample) consisting of NWs, which, based on the structural characterization, are formed through a transition to $CsPbBr_3$ tetragonal phase. Compared to the 3D $CsPbBr_3$ nanocubes, the 1D NW structures formed upon addition of Olam at low concentration (0.075mmol/mL) can be described as originated through a 3D distortion mechanism: due to Olam-induced $PbBr_2$ depletion, the $[PbBr_6]^{4-}$ octahedra start to be disconnected and reordered into linear chains extended along the *c* axis of the tetragonal lattice. These 1D nanostructures very poorly emitting and poorly stable convert into a completely photo-inactive non perovskite structures after 1 week.

While the specific affinity of Olam for NC surface ions explains the induced $PbBr_2$ depletion and transformation of 3D nanocubes into 1D tetragonal $CsPbBr_3$ perovskite and 0D Cs_4PbBr_6 nanostructures, the decrease in the pH can be regarded as the driving force [12-14] that transforms nanocubes into size tuneable NPLs.

In this regards, the formation of NPLs during the synthesis has been already described in literature to be favored over nanocubes by the presence of alkyl carboxylic acid [14, 15, 17] or, similarly, by dropping inorganic bromidic acid [12, 21]. The acid-base equilibrium [14] between the organic (inorganic) acid and alkyl amine, which is an organic base, used as ligand in the reaction mixture, generates alkylammonium. The excess of alkyl ammonium has been demonstrated to compete with the Cs^+ ions at the surface [47] during the growing step and selectively slows down the growth along these directions, blocking specific surface sites, resulting in anisotropic NPLs.

Similarly, here, the pH decrease, upon post-synthesis addition of fresh Olac, effectively control the morphological evolution of the as prepared nanocubes into NPLs. The organic carboxylic acid shifts the Bronsted-Lowry equilibrium between the two Olam/Olac free ligands, promoting the protonation of Olam in solution and the formation of oleylammonium cation, $Olam^+$. The alkylammonium cation may be also generated in situ by protonation of Olam stabilizing the NC surface that, only loosely bound, can be easily detached upon pH decrease.

It has been reported that, although alkyl ammonium ions bind more weakly compared to carboxylates, they are more effective in tuning the growth of anisotropic platelet, along that surface not involved in alkyl ammonium substitution. Therefore, the in situ generated $Olam^+$ controls the changes of the morphologies and the growth NPL structures. $Olam^+$ may either substitute the surface Cs^+ [21], thus partially changing the nanocrystals stoichiometry resulting in $Cs_{1-x}(Olam)_xPbBr_3$, either intercalates in the 3D nanostructure. Since $Olam^+$ (alkyl chain length nearly 2 nm) is larger than Cs^+ (ionic radius 167 pm) it cannot fit into the rigid 3D perovskite structures and the system split into layers of lower dimensional network (2D) [48]. Although this substitution is thermodynamically not favoured, still the TEM micrographs of Olac 75 (Figure 4) provide a clear evidence of the formation of 2D

nanostructures, 4 nm thick (nearly 3 multilayers), hence in quantum confinement regime, smaller than the as-prepared nanocubes (8 nm in later size). This morphological finding confirms the feasibility of fragmentation induced by in situ originated $Olam^+$, which is also corroborated by the spectroscopic characterization reported in Figure 5 that shows blue shifted exciton absorption and PL feature. Meanwhile, the overall process results in a general increase in the NPLs lateral size that can even reach tens of nanometres, revealing that $Olam^+$ substitution and induced fragmentation is accompanied by surfactant controlled recrystallization phenomena. The θ/2θ XRD pattern reported in Figure 6f, closely matching that of the orthorhombic phase, highlights that the 002 and 110 (and similarly 004 and 220) represent the growing directions involved in the increased lateral size of the NPLs. Interesting, the lateral size of the NPLs becomes even larger, with nanostructures preferring a face-on assembly on the TEM surface (Figure 4c) either as the Olac concentration increases (Olac 150 sample), thus the pH decreases, or by ageing the Olac 75 samples. We can, thus, conclude that fragmentation and reorganization/recrystallization into larger nanostructures is kinetically controlled by pH and can be slowed down by decreasing the concentration of added Olac. Such a multistep mechanism that involves a pH decrease due to Olac addition and the formation of $Olam^+$ that controls the anisotropic growth, through cesium ions substitution and NC surface binding, is also demonstrated by structural characterization (Figure 7c). The θ/2θ XRD pattern of Olac 150 sample shows (Figure 7c) a sharp reflection at 11.6° that can be ascribed to Cs_3O (Figure 6e reference pattern), proving the Cs^+ release in solution. Since the Cs ions, responsible of the NPL lateral size growth, are not completely consumed in recrystallization process, the nanostructure becomes prone to air oxidation.

4. Conclusions

The study has established the key role played by ligands in the destabilization of $CsPbBr_3$ nanocubes upon oleyl amine and oleic acid addition, dilution and ageing. The mechanism driving the observed transformations has been depicted thanks to a comprehensive morphological, spectroscopic and structural characterization. In particular the acid/base equilibrium between the two ligands acting as

Lewis acid and base and/or the affinity of oleylammonium for lead halide have been demonstrated to promote the transformation of nanocubes into 2D NPLs, with tunable thickness and lateral size, or 1D NWs and 0D non perovskite rhombohedral nanostructures, upon oleic acid or oleyl ammine addition, respectively. Concomitantly, the dynamic between adsorbed and free ligands in solution and ligand solubility in non-polar solvent have been proven to induce fragmentation phenomena due to osmotic solvent swelling, resulting in the formation of smaller 3D and 2D nanostructures. Conversely, the low $CsPbBr_3$ energy formation, which makes the surfactant controlled recrystallization of free ions in solution a viable process at room temperature, results in an increase in the average size of the nanostructures. As a matter of the fact, in order to protect $CsPbBr_3$ integrity and prevent structural, morphological and spectroscopic variations, all these equilibria need to be taken into account during processing of this material. This work demonstrates that a truly integrated investigation approach is able to provide original and unique findings essential for the fundamental understanding of the issues related to cesium lead halide perovskite stability, but also relevant for properly exploiting the potential of this type of material in technological applications

Acknowledgements

This work was financially supported by the MIUR PRIN 2015 no. 2015XBZ5YA, the Project of Industrial Research PON Best4y ARS01_00519 and the project FIRB Futuro in Ricerca no. RBFR122HFZ. The authors thank PON SISTEMA no. PONa3_00369 for feasibility of using UV-Vis-NIR Spectrophotometer. Rocco Lassandro is acknowledged for his technical support in the X-Ray laboratory.

References

[1] Protesescu, L.;Yakunin, S.;Bodnarchuk, M. I.;Krieg, F.;Caputo, R.;Hendon, C. H.;Yang, R. X.;Walsh, A.;Kovalenko, M. V. Nanocrystals of Cesium Lead Halide Perovskites (CsPbX3, X = Cl,

Br, and I): Novel Optoelectronic Materials Showing Bright Emission with Wide Color Gamut. *Nano Lett.* 2015, *15*, 3692-3696.

[2] Ha, S.-T.;Su, R.;Xing, J.;Zhang, Q.;Xiong, Q. Metal halide perovskite nanomaterials: synthesis and applications. *Chemical Science* 2017, *8*, 2522-2536.

[3] Kovalenko, M. V.;Protesescu, L.;Bodnarchuk, M. I. Properties and potential optoelectronic applications of lead halide perovskite nanocrystals. *Science* 2017, *358*, 745-750.

[4] Huang, H.;Bodnarchuk, M. I.;Kershaw, S. V.;Kovalenko, M. V.;Rogach, A. L. Lead Halide Perovskite Nanocrystals in the Research Spotlight: Stability and Defect Tolerance. *ACS Energy Letters* 2017, *2*, 2071-2083.

[5] Liu, Q.;Wang, Y.;Sui, N.;Wang, Y.;Chi, X.;Wang, Q.;Chen, Y.;Ji, W.;Zou, L.;Zhang, H. Exciton Relaxation Dynamics in Photo-Excited CsPbI3 Perovskite Nanocrystals. *Scientific Reports* 2016, *6*, 29442.

[6] Liao, J.-F.;Li, W.-G.;Rao, H.-S.;Chen, B.-X.;Wang, X.-D.;Chen, H.-Y.;Kuang, D.-B. Inorganic cesium lead halide CsPbX3 nanowires for long-term stable solar cells. *Science China Materials* 2017, *60*, 285-294.

[7] Li, B.;Zhang, Y.;Fu, L.;Yu, T.;Zhou, S.;Zhang, L.;Yin, L. Surface passivation engineering strategy to fully-inorganic cubic CsPbI3 perovskites for high-performance solar cells. *Nature Communications* 2018, *9*, 1076.

[8] Zhang, D.;Yu, Y.;Bekenstein, Y.;Wong, A. B.;Alivisatos, A. P.;Yang, P. Ultrathin Colloidal Cesium Lead Halide Perovskite Nanowires. *J. Am. Chem. Soc.* 2016, *138*, 13155-13158.

[9] Kim, Y.;Yassitepe, E.;Voznyy, O.;Comin, R.;Walters, G.;Gong, X.;Kanjanaboos, P.;Nogueira, A. F.;Sargent, E. H. Efficient Luminescence from Perovskite Quantum Dot Solids. *ACS Appl. Mater. Interfaces* 2015, *7*, 25007-25013.

[10] Reichardt, C. *Solvents and Solvent Effects in Organic Chemistry* WILEY-VCH Verlag GmbH & Co. KGaA: Weinheim, Germany, 2006.

[11] De Roo, J.;Ibáñez, M.;Geiregat, P.;Nedelcu, G.;Walravens, W.;Maes, J.;Martins, J. C.;Van Driessche, I.;Kovalenko, M. V.;Hens, Z. Highly Dynamic Ligand Binding and Light Absorption Coefficient of Cesium Lead Bromide Perovskite Nanocrystals. *ACS Nano* 2016, *10*, 2071-2081.

[12] Udayabhaskararao, T.;Kazes, M.;Houben, L.;Lin, H.;Oron, D. Nucleation, Growth, and Structural Transformations of Perovskite Nanocrystals. *Chem. Mater.* 2017, *29*, 1302-1308.

[13] Cho, J.;Jin, H.;Sellers, D. G.;Watson, D. F.;Son, D. H.;Banerjee, S. Influence of ligand shell ordering on dimensional confinement of cesium lead bromide (CsPbBr3) perovskite nanoplatelets. *Journal of Materials Chemistry C* 2017, *5*, 8810-8818.

[14] Almeida, G.;Goldoni, L.;Akkerman, Q.;Dang, Z.;Khan, A. H.;Marras, S.;Moreels, I.;Manna, L. Role of Acid–Base Equilibria in the Size, Shape, and Phase Control of Cesium Lead Bromide Nanocrystals. *ACS Nano* 2018, *12*, 1704-1711.

[15] Pan, A.;He, B.;Fan, X.;Liu, Z.;Urban, J. J.;Alivisatos, A. P.;He, L.;Liu, Y. Insight into the Ligand-Mediated Synthesis of Colloidal CsPbBr3 Perovskite Nanocrystals: The Role of Organic Acid, Base, and Cesium Precursors. *ACS Nano* 2016, *10*, 7943-7954.

[16] Liang, Z.;Zhao, S.;Xu, Z.;Qiao, B.;Song, P.;Gao, D.;Xu, X. Shape-Controlled Synthesis of All-Inorganic CsPbBr3 Perovskite Nanocrystals with Bright Blue Emission. *ACS Appl. Mater. Interfaces* 2016, *8*, 28824-28830.

[17] Shamsi, J.;Dang, Z.;Bianchini, P.;Canale, C.;Di Stasio, F.;Brescia, R.;Prato, M.;Manna, L. Colloidal Synthesis of Quantum Confined Single Crystal CsPbBr3 Nanosheets with Lateral Size Control up to the Micrometer Range. *J. Am. Chem. Soc.* 2016, *138*, 7240-7243.

[18] Lignos, I.;Protesescu, L.;Emiroglu, D. B.;Maceiczyk, R.;Schneider, S.;Kovalenko, M. V.;deMello, A. J. Unveiling the Shape Evolution and Halide-Ion-Segregation in Blue-Emitting Formamidinium Lead Halide Perovskite Nanocrystals Using an Automated Microfluidic Platform. *Nano Lett.* 2018, *18*, 1246-1252.

[19] Goodwin, C. A. P.;Reta, D.;Ortu, F.;Chilton, N. F.;Mills, D. P. Synthesis and Electronic Structures of Heavy Lanthanide Metallocenium Cations. *J. Am. Chem. Soc.* 2017, *139*, 18714-18724.

[20] Zhang, D.;Eaton, S. W.;Yu, Y.;Dou, L.;Yang, P. Solution-Phase Synthesis of Cesium Lead Halide Perovskite Nanowires. *J. Am. Chem. Soc.* 2015, *137*, 9230-9233.

[21] Akkerman, Q. A.;Motti, S. G.;Srimath Kandada, A. R.;Mosconi, E.;D'Innocenzo, V.;Bertoni, G.;Marras, S.;Kamino, B. A.;Miranda, L.;De Angelis, F.;Petrozza, A.;Prato, M.;Manna, L. Solution Synthesis Approach to Colloidal Cesium Lead Halide Perovskite Nanoplatelets with Monolayer-Level Thickness Control. *J. Am. Chem. Soc.* 2016, *138*, 1010-1016.

[22] Seth, S.;Samanta, A. A Facile Methodology for Engineering the Morphology of CsPbX3 Perovskite Nanocrystals under Ambient Condition. *Scientific Reports* 2016, *6*, 37693.

[23] Sun, S.;Yuan, D.;Xu, Y.;Wang, A.;Deng, Z. Ligand-Mediated Synthesis of Shape-Controlled Cesium Lead Halide Perovskite Nanocrystals via Reprecipitation Process at Room Temperature. *ACS Nano* 2016, *10*, 3648-3657.

[24] Xiaoming, L.;Ye, W.;Shengli, Z.;Bo, C.;Yu, G.;Jizhong, S.;Haibo, Z. CsPbX3 Quantum Dots for Lighting and Displays: Room-Temperature Synthesis, Photoluminescence Superiorities, Underlying Origins and White Light-Emitting Diodes. *Adv. Funct. Mater.* 2016, *26*, 2435-2445.

[25] Ramasamy, P.;Lim, D.-H.;Kim, B.;Lee, S.-H.;Lee, M.-S.;Lee, J.-S. All-inorganic cesium lead halide perovskite nanocrystals for photodetector applications. *Chem. Commun.* 2016, *52*, 2067-2070.

[26] Doane, T. L.;Ryan, K. L.;Pathade, L.;Cruz, K. J.;Zang, H.;Cotlet, M.;Maye, M. M. Using Perovskite Nanoparticles as Halide Reservoirs in Catalysis and as Spectrochemical Probes of Ions in Solution. *ACS Nano* 2016, *10*, 5864-5872.

[27] Krieg, F.;Ochsenbein, S. T.;Yakunin, S.;ten Brinck, S.;Aellen, P.;Süess, A.;Clerc, B.;Guggisberg, D.;Nazarenko, O.;Shynkarenko, Y.;Kumar, S.;Shih, C.-J.;Infante, I.;Kovalenko, M.

V. Colloidal CsPbX3 (X = Cl, Br, I) Nanocrystals 2.0: Zwitterionic Capping Ligands for Improved Durability and Stability. *ACS Energy Letters* 2018, *3*, 641-646.

[28] Swarnkar, A.;Marshall, A. R.;Sanehira, E. M.;Chernomordik, B. D.;Moore, D. T.;Christians, J. A.;Chakrabarti, T.;Luther, J. M. Quantum dot–induced phase stabilization of α-CsPbI₃ perovskite for high-efficiency photovoltaics. *Science* 2016, *354*, 92-95.

[29] Akkerman, Q. A.;Abdelhady, A. L.;Manna, L. Zero-Dimensional Cesium Lead Halides: History, Properties, and Challenges. *J. Phys. Chem. Lett.* 2018, *9*, 2326-2337.

[30] Palazon, F.;Almeida, G.;Akkerman, Q. A.;De Trizio, L.;Dang, Z.;Prato, M.;Manna, L. Changing the Dimensionality of Cesium Lead Bromide Nanocrystals by Reversible Postsynthesis Transformations with Amines. *Chem. Mater.* 2017, *29*, 4167-4171.

[31] Akkerman, Q. A.;Park, S.;Radicchi, E.;Nunzi, F.;Mosconi, E.;De Angelis, F.;Brescia, R.;Rastogi, P.;Prato, M.;Manna, L. Nearly Monodisperse Insulator Cs4PbX6 (X = Cl, Br, I) Nanocrystals, Their Mixed Halide Compositions, and Their Transformation into CsPbX3 Nanocrystals. *Nano Lett.* 2017, *17*, 1924-1930.

[32] Liu, Z.;Bekenstein, Y.;Ye, X.;Nguyen, S. C.;Swabeck, J.;Zhang, D.;Lee, S.-T.;Yang, P.;Ma, W.;Alivisatos, A. P. Ligand Mediated Transformation of Cesium Lead Bromide Perovskite Nanocrystals to Lead Depleted Cs4PbBr6 Nanocrystals. *J. Am. Chem. Soc.* 2017, *139*, 5309-5312.

[33] Udayabhaskararao, T.;Houben, L.;Cohen, H.;Menahem, M.;Pinkas, I.;Avram, L.;Wolf, T.;Teitelboim, A.;Leskes, M.;Yaffe, O.;Oron, D.;Kazes, M. A Mechanistic Study of Phase Transformation in Perovskite Nanocrystals Driven by Ligand Passivation. *Chem. Mater.* 2018, *30*, 84-93.

[34] de Weerd, C.;Lin, J.;Gomez, L.;Fujiwara, Y.;Suenaga, K.;Gregorkiewicz, T. Hybridization of Single Nanocrystals of Cs4PbBr6 and CsPbBr3. *J. Phys. Chem. C* 2017, *121*, 19490-19496.

[35] Haiming, Z.;Tuan, T. M.;Jue, W.;Yongping, F.;P., J. P.;Kiyoshi, M.;Song, J.;X.-Y., Z. Organic Cations Might Not Be Essential to the Remarkable Properties of Band Edge Carriers in Lead Halide Perovskites. *Adv. Mater.* 2017, *29*, 1603072.

[36] Eperon, G. E.;Ginger, D. S. B-Site Metal Cation Exchange in Halide Perovskites. *ACS Energy Letters* 2017, *2*, 1190-1196.

[37] Bekenstein, Y.;Koscher, B. A.;Eaton, S. W.;Yang, P.;Alivisatos, A. P. Highly Luminescent Colloidal Nanoplates of Perovskite Cesium Lead Halide and Their Oriented Assemblies. *J. Am. Chem. Soc.* 2015, *137*, 16008-16011.

[38] Di Stasio, F.;Imran, M.;Akkerman, Q. A.;Prato, M.;Manna, L.;Krahne, R. Reversible Concentration-Dependent Photoluminescence Quenching and Change of Emission Color in CsPbBr3 Nanowires and Nanoplatelets. *J. Phys. Chem. Lett.* 2017, *8*, 2725-2729.

[39] Vikash Kumar, R.;Abhishek, S.;Rayan, C.;Angshuman, N. Excellent green but less impressive blue luminescence from CsPbBr 3 perovskite nanocubes and nanoplatelets. *Nanotechnology* 2016, *27*, 325708.

[40] Lv, L.;Xu, Y.;Fang, H.;Luo, W.;Xu, F.;Liu, L.;Wang, B.;Zhang, X.;Yang, D.;Hu, W.;Dong, A. Generalized colloidal synthesis of high-quality, two-dimensional cesium lead halide perovskite nanosheets and their applications in photodetectors. *Nanoscale* 2016, *8*, 13589-13596.

[41] Palazon, F.;Urso, C.;De Trizio, L.;Akkerman, Q.;Marras, S.;Locardi, F.;Nelli, I.;Ferretti, M.;Prato, M.;Manna, L. Postsynthesis Transformation of Insulating Cs4PbBr6 Nanocrystals into Bright Perovskite CsPbBr3 through Physical and Chemical Extraction of CsBr. *ACS Energy Letters* 2017, *2*, 2445-2448.

[42] Imran, M.;Di Stasio, F.;Dang, Z.;Canale, C.;Khan, A. H.;Shamsi, J.;Brescia, R.;Prato, M.;Manna, L. Colloidal Synthesis of Strongly Fluorescent CsPbBr3 Nanowires with Width Tunable down to the Quantum Confinement Regime. *Chem. Mater.* 2016, *28*, 6450-6454.

[43] Tong, Y.;Ehrat, F.;Vanderlinden, W.;Cardenas-Daw, C.;Stolarczyk, J. K.;Polavarapu, L.;Urban, A. S. Dilution-Induced Formation of Hybrid Perovskite Nanoplatelets. *ACS Nano* 2016, *10*, 10936-10944.

[44] Sichert, J. A.;Tong, Y.;Mutz, N.;Vollmer, M.;Fischer, S.;Milowska, K. Z.;García Cortadella, R.;Nickel, B.;Cardenas-Daw, C.;Stolarczyk, J. K.;Urban, A. S.;Feldmann, J. Quantum Size Effect in Organometal Halide Perovskite Nanoplatelets. *Nano Lett.* 2015, *15*, 6521-6527.

[45] de Weerd, C.;Gomez, L.;Zhang, H.;Buma, W. J.;Nedelcu, G.;Kovalenko, M. V.;Gregorkiewicz, T. Energy Transfer between Inorganic Perovskite Nanocrystals. *J. Phys. Chem. C* 2016, *120*, 13310-13315.

[46] Protesescu, L.;Yakunin, S.;Nazarenko, O.;Dirin, D. N.;Kovalenko, M. V. Low-Cost Synthesis of Highly Luminescent Colloidal Lead Halide Perovskite Nanocrystals by Wet Ball Milling. *ACS Applied Nano Materials* 2018, *1*, 1300-1308.

[47] Ravi, V. K.;Santra, P. K.;Joshi, N.;Chugh, J.;Singh, S. K.;Rensmo, H.;Ghosh, P.;Nag, A. Origin of the Substitution Mechanism for the Binding of Organic Ligands on the Surface of CsPbBr3 Perovskite Nanocubes. *J. Phys. Chem. Lett.* 2017, *8*, 4988-4994.

[48] Boix, P. P.;Agarwala, S.;Koh, T. M.;Mathews, N.;Mhaisalkar, S. G. Perovskite Solar Cells: Beyond Methylammonium Lead Iodide. *J. Phys. Chem. Lett.* 2015, *6*, 898-907.